ACS OMEGA

http://pubs.acs.org/journal/acsodf

Article

Impact of H_2O on the Adsorption of Hg^0 on Activated Carbon

Julian Steinhaus,* Christoph Pasel, Christian Bläker, and Dieter Bathen

Cite This: *ACS Omega* 2021, 6, 16989−17001

Read Online

ACCESS | Metrics & More | Article Recommendations | Supporting Information

ABSTRACT: In this work, the influence of water on the adsorption of mercury is systematically investigated on basic and washed activated carbons. Breakthrough curves were measured and temperature-programmed desorption (TPD) experiments were performed with mercury and water. Both physisorptive and chemisorptive interactions are relevant in the adsorption of mercury. The experiments show that the presence of water in the pores promotes chemisorption of mercury on washed activated carbons while there is little influence on chemisorption on basic materials. Washing exposes or forms oxygen functional groups that are chemisorptive sites for mercury. Obviously, effective chemisorption of mercury requires both the presence of water and of oxygen functional groups. As mercury chemisorption is preceded by a physisorptive step, higher physisorptive mercury loading at lower temperature (30 °C) enhances chemisorption though the reaction rate constant is smaller than at higher temperature (100 °C). Sequential adsorption and partial desorption of water at lower temperature changes the surface chemistry without inhibiting mercury physisorption. Here, the highest chemisorption rates were found. The number of desorption peaks in the TPD experiments corresponds to the number of adsorption and desorption mechanisms with different oxygen functional groups in the presence of water. The results of the TPD experiments were simulated using a transport model extended by an approach for chemisorption. The simulation results provide reaction parameters (activation energy, frequency factor, and reaction order) of each mechanism. As in many heterogeneously catalyzed reactions, the activation energy and the frequency factor are independent of mercury loading and increase with increasing temperature.

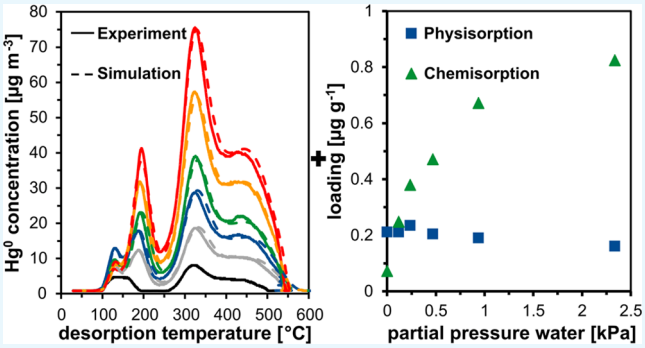

1. INTRODUCTION

The toxic effect of mercury on humans and the environment makes reduction in air, water, and soil a goal of national and international efforts. Established separation processes for mercury removal, such as adsorption by entrained flow adsorbers[1−4] or absorption by scrubbers[5,6] are mainly suitable for removal from large continuous waste gas streams. Small discontinuous waste gas streams can be efficiently treated from a technical and economic point of view by fixed-bed adsorption with impregnated[7−17] and nonimpregnated[18−29] activated carbons. For the design of adsorbers and optimization of operating conditions, a precise knowledge of adsorption mechanisms is necessary.

Mercury is emitted in elemental and oxidized forms during combustion processes. Since elemental mercury (Hg^0) is present in significant amounts in flue gas due to its high volatility and adsorbs worse than oxidized mercury (e.g., mercuric chloride),[30] the focus of this work is on the investigation of the adsorption of elemental mercury. The literature shows that both physisorptive and chemisorptive interactions are important for adsorption of elemental mercury on activated carbons. The chemisorptive separation of mercury by impregnated activated carbons is widely used in technical applications. However, nonimpregnated activated carbons also form chemisorptive interactions with mercury. Precise knowledge of the interactions that occur is of great interest to both science and technology.

In previous publications,[31,32] we have extensively reviewed the literature on physisorptive and chemisorptive single-component adsorption of Hg^0. Mercury can react chemisorptively with surface groups of activated carbons in the presence of other components such as water, oxygen, sulfur, or chlorine.[10,11,19,33−37] As the influence of water is of particular importance, in the following, the current state of research on the impact of water on the adsorption of Hg^0 on nonimpregnated activated carbons is described.

Li et al.[33] performed coupled adsorption and desorption experiments on dried and water-loaded activated carbons. The experiments with temperature-programmed desorption showed that water promotes chemisorption of mercury. The authors suggested an interaction of water with oxygen functional

Received: April 14, 2021
Accepted: June 4, 2021
Published: June 24, 2021

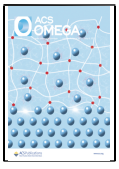

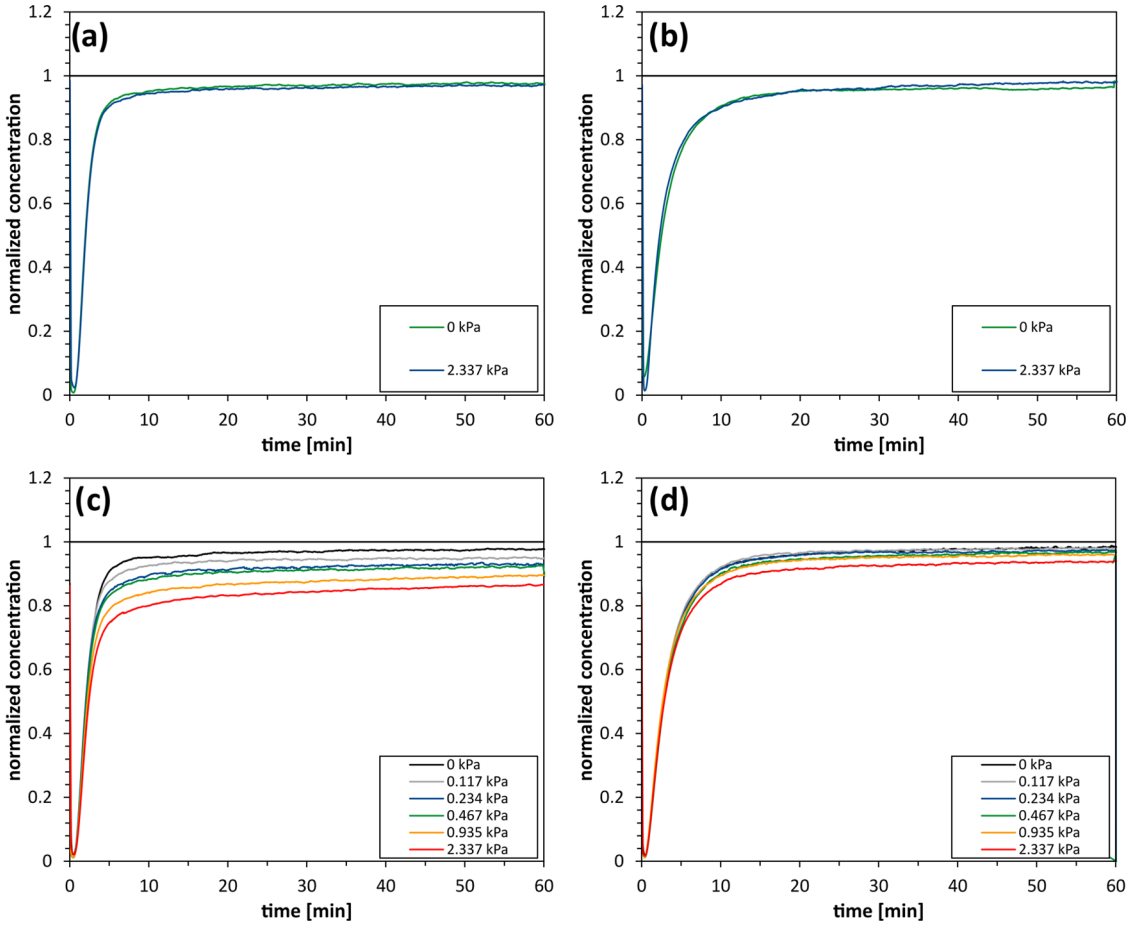

Figure 1. Breakthrough curves of Hg^0 at 100 °C with 264 $\mu g\ m^{-3}$ and a water partial pressure from 0 to 2.337 kPa on the basic activated carbons AC 01 (a) and AC 02 (b) as well as on the activated carbons washed with water AC 01 (c) and AC 02 (d).

groups, by which the adsorption of Hg^0 is favored. The nature of the surface groups and their interactions with water are not further discussed.

Yan et al.[38] used single breakthrough curves on five activated carbons to prove that increasing the relative humidity to 80% can reduce the adsorption capacity to a quarter. The breakthrough curves were recorded at an adsorption temperature of 90 °C, a mercury concentration of 10 $\mu g\ m^{-3}$, and an oxygen content of 6 vol %.

Liu et al.[39] published adsorption experiments with a mercury concentration of 55 $\mu g\ m^{-3}$ at a temperature of 140 °C. They showed that a relative humidity of 5% had no effect on mercury adsorption. Above a relative humidity of 10%, the micropores of the activated carbon filled with water, blocking adsorption sites and decreasing the adsorption capacity.

Lopez-Anton et al.[40,41] used breakthrough curves to investigate the adsorption of mercury from an exhaust gas on activated carbons. The presence of water in the waste gas caused a reduction in mercury adsorption.

Rafeen et al.[42] examined mercury adsorption from a moist gas stream on $CuCl_2$-impregnated activated carbons using breakthrough curves. The experiments were executed at the saturated vapor pressure of water at 20 °C and a mercury concentration of 2000 $\mu g\ m^{-3}$. The authors assume that the adsorption of mercury is inhibited by capillary condensation of water. Similar results were published by Hsi et al.[43] on sulfur-impregnated activated carbons.

Hu et al.[44] performed experiments with a simulated exhaust gas consisting of CO_2, SO_2, Cl_2, HCl, H_2O, O_2, and Hg^0 to study the catalytic oxidation of elemental mercury. The authors suppose that high water concentrations inhibit mercury oxidation by reducing the conversion of HCl to chlorine atoms that oxidize mercury. The presence of SO_2 and water also leads to the consumption of Cl atoms, thereby restraining mercury oxidation.

Wang et al.[45] studied the effect of water on the adsorption and oxidation of mercury from a carrier gas (O_2 + CO_2) on activated carbons. Increasing the water content hindered mercury adsorption. The authors suggest that water blocked the micropores of the activated carbon. Additionally, water is assumed to provide additional electrons on the surface of the activated carbon so that Hg^{2+} is reduced to Hg^0. TPD experiments proved that the adsorbed mercury complexes are not altered by water in the gas phase.

The literature shows that water has an impact on the adsorption of elemental mercury on activated carbons. While some authors observed capacity increasing influence of water, other authors reported a capacity reduction in the presence of water, however, the underlying mechanisms are not yet understood. Therefore, the Chair of Thermal Process Engineering at the University of Duisburg-Essen investigates the influence of water on the adsorption of Hg^0 on activated carbons. This article systematically examines whether only water in the gas phase is required for significant chemisorption of mercury or oxygen functional groups must be present on the

https://doi.org/10.1021/acsomega.1c01994
ACS Omega 2021, 6, 16989−17001

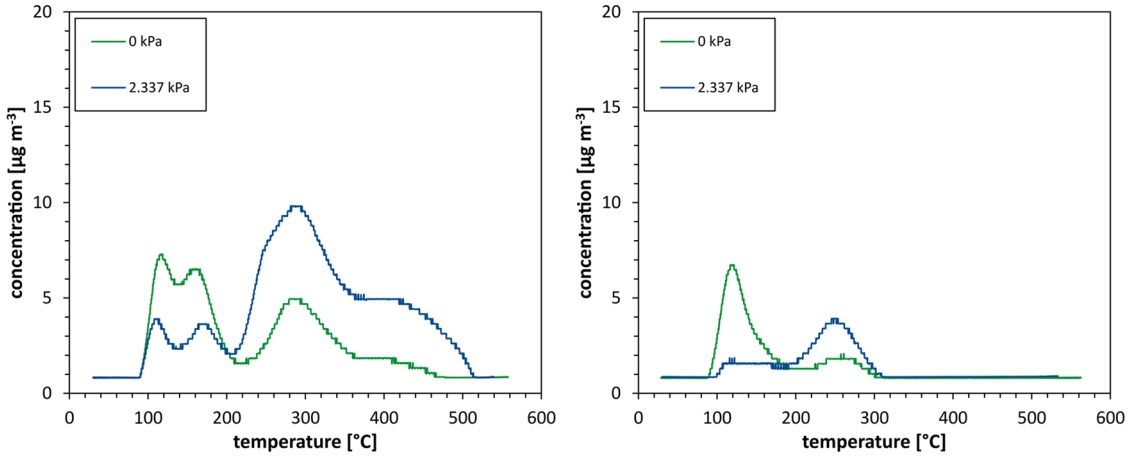

Figure 2. Hg^0 concentrations in TPD experiments on basic activated carbons AC 01 (left) and AC 02 (right) after Hg^0 loading at 100 °C for 1 h at a water partial pressure range between 0 and 2.337 kPa.

surface of the activated carbon in addition to the water in the gas phase. Also, the interference of physisorbed water with the physisorptive adsorption of mercury is considered, which occurs before chemisorption. For that purpose, mercury adsorption experiments with different amounts of water in the gas phase at different temperatures on basic and washed activated carbons were conducted.

Furthermore, it is studied whether different mechanisms are involved in the chemisorption of mercury with water, leading to bonds of different energetic value that would be expected for the chemisorption of mercury with different oxygen functional groups. Coupled adsorption and desorption experiments with Hg^0 were performed on activated carbons to investigate these issues.

2. RESULTS AND DISCUSSION

2.1. Influence of Water on the Dynamics of Hg^0 Adsorption. Figure 1 shows experimental breakthrough curves of the adsorption of elemental mercury with water in the gas phase at 100 °C on AC 01 (a) and AC 02 (b), and on washed activated carbons AC 01 (c) and AC 02 (d). The mercury concentration was kept constant at 264 $\mu g\ m^{-3}$. The partial pressures of water were 0 kPa, 0.117 kPa (φ_W = 0.116%), 0.234 kPa (φ_W = 0.231%), 0.467 kPa (φ_W = 0.461%), 0.935 kPa (φ_W = 0.923%), and 2.337 kPa (φ_W = 2.307%).

The breakthrough curves of the basic activated carbons have an early breakthrough and a subsequent rapid increase in concentration. After about 20 min, nearly no more increase of the concentration is observed. The concentrations in this state are slightly below the input concentration. This indicates that there are very slow chemisorption reactions of mercury, which only have a minor influence on adsorption. A comparison of the concentration curves at 0 and 2.337 kPa of water shows no significant effect of water in the gas phase on the adsorption of elemental mercury. The breakthrough curves measured on the activated carbons washed with water also exhibit an almost instantaneous breakthrough and a rapid increase in concentration. As the experiment progresses, the slopes of the concentration curves decrease significantly, so that in the experiments with water in the gas phase, no state with nearly constant concentrations is reached within the specified experimental time. The very slow kinetics of the adsorption mechanism at high water partial pressures indicates chemisorptive interactions between Hg^0, water, and the activated carbon surface.

2.2. Temperature-Programmed Desorption of Hg^0. For detailed investigation of the mechanisms, concentration swing desorption (CSA) and TPD experiments were performed after the adsorption step. The basic activated carbons were first loaded with a mercury concentration of 264 $\mu g\ m^{-3}$ at 100 °C for a period of 1 h. CSA was used to desorb the physisorptively bound mercury. Subsequently, the temperature was increased with a ramp of 5 °C min^{-1} (TPD) to desorb the chemisorptively bound mercury. Figure 2 presents the concentration curves of the desorbed Hg^0 in $\mu g\ m^{-3}$ as a function of temperature in °C for the basic activated carbons AC 01 (left) and AC 02 (right) with a water partial pressure of 0 and 2.337 kPa for the TPD experiments.

Table 1 gives the loadings and mass ratios of the coupled adsorption and desorption tests with CSA and TPD.

Table 1. Mercury Loadings and Mass Ratios of Coupled Adsorption and Desorption Experiments at Water Partial Pressures of 0 and 2.337 kPa at 100 °C on Basic Activated Carbons AC 01 and AC 02

		loading of Hg^0			
activated carbon	water partial pressure [kPa]	Ads. [$\mu g\ g^{-1}$]	CSA [$\mu g\ g^{-1}$]	TPD [$\mu g\ g^{-1}$]	mass ratio $\frac{x_{CSA}+x_{TPD}}{x_{Ads}}$
AC 01	0	0.238	0.204	0.058	1.10
	2.337	0.237	0.158	0.101	1.09
AC 02	0	0.336	0.335	0.023	1.06
	2.337	0.335	0.308	0.018	0.97

From the calculated loadings of adsorption, CSA and TPD (Table 1), it is clear that physisorption is the dominant mechanism. The chemisorptive fraction is significantly lower than the physisorptive fraction. Water in the gas phase does not affect the total amount of Hg^0 adsorbed. The ratio of desorbed to adsorbed mass is close to 1, so that desorption in TPD occurs entirely in the form of Hg^0.

The concentration curves of the TPD experiments (Figure 2) show distinctive desorption peaks, each assigned to a chemisorptive adsorption mechanism. The peak height is very low with a maximum concentration of 10 $\mu g\ m^{-3}$. In the presence of water in the gas phase, Hg^0 preferentially occupies

https://doi.org/10.1021/acsomega.1c01994
ACS Omega 2021, 6, 16989−17001

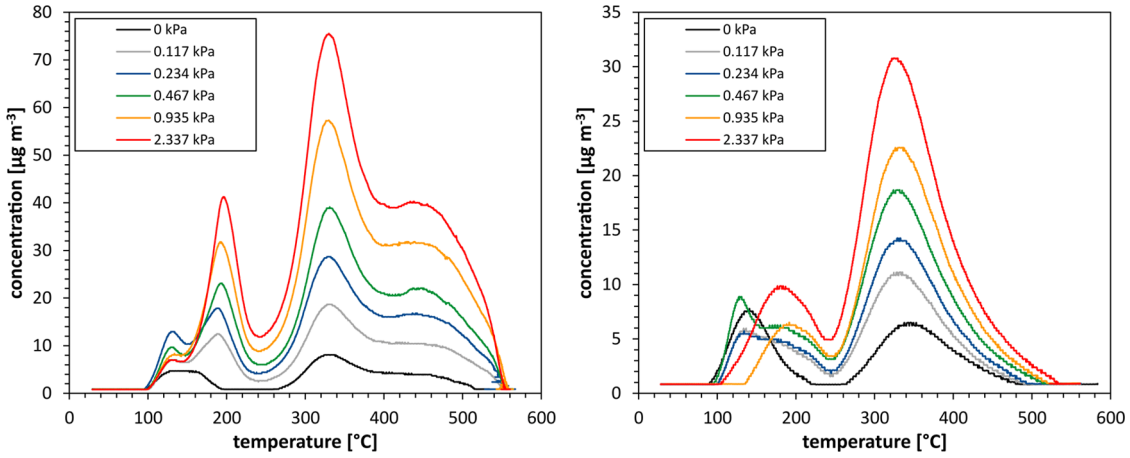

Figure 3. Hg^0 concentrations in TPD experiments on washed activated carbons AC 01 (left) and AC 02 (right) after Hg^0 loading at 100 °C for 1 h at a water partial pressure range between 0 and 2.337 kPa.

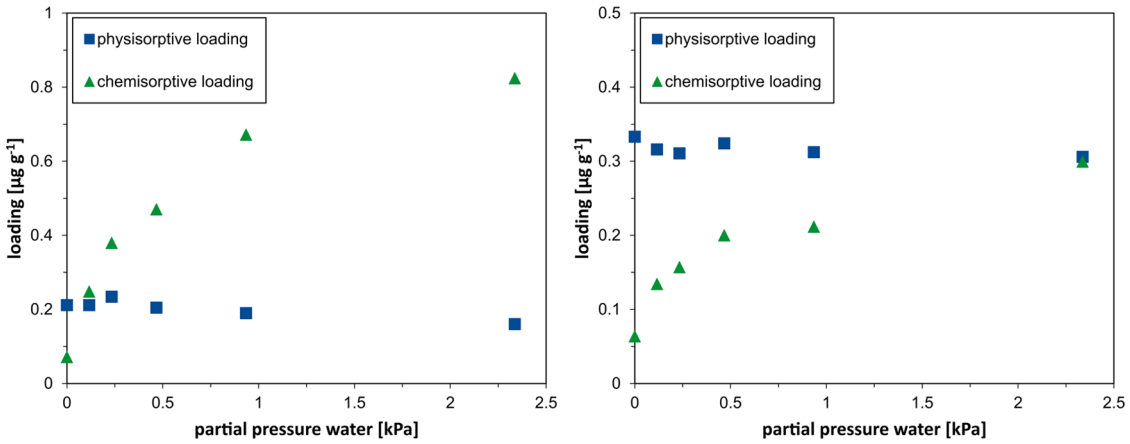

Figure 4. Desorbed loading of Hg^0 during CSA and TPD experiments for washed activated carbons AC 01 (left) and AC 02 (right).

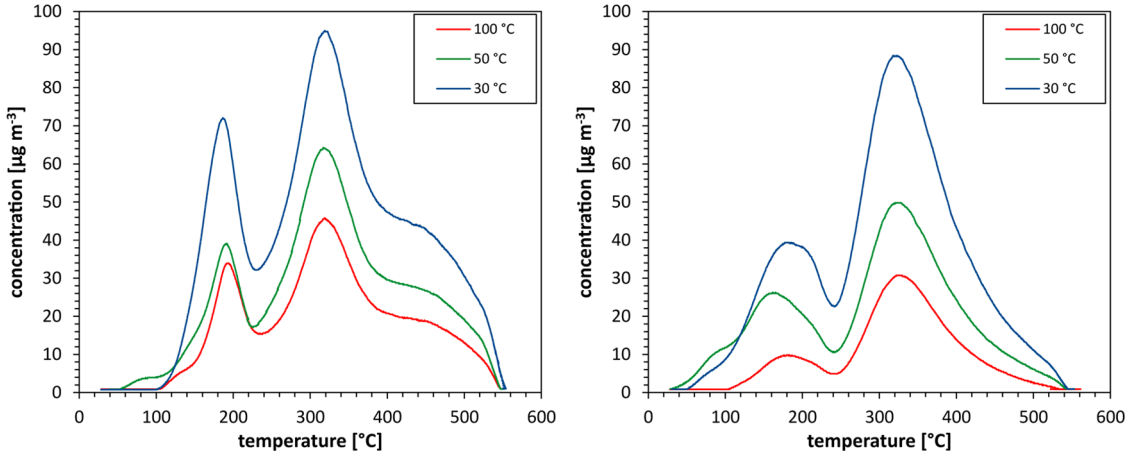

Figure 5. Hg^0 concentrations in TPD experiments on washed activated carbons AC 01 (left) and AC 02 (right) after adsorption at temperatures of 30, 50, and 100 °C at a water partial pressure of 2.337 kPa.

the adsorption sites of high energetic value, which are only desorbed at higher temperatures. In the case of activated carbon AC 01, a larger part of the mercury is chemisorptively bound due to this effect, while only a slight change is observed in the activated carbon AC 02 (see also Table 1).

Figure 3 illustrates the mercury concentrations in TPD experiments on the washed activated carbons AC 01 (left) and AC 02 (right) at different water partial pressures. The calculated loadings of physisorptively and chemisorptively bound mercury are plotted in Figure 4.

The desorption curves of the TPD experiments show three and four peaks, respectively, with maximum concentrations at temperatures of approximately 125, 195, 330, and 450 °C (Figure 3). The concentration curves of the TPD experiments

https://doi.org/10.1021/acsomega.1c01994
ACS Omega 2021, 6, 16989−17001

as well as the calculated loadings (Figure 4) prove that chemisorption is enhanced by increasing the water content in the gas phase. Water isotherms of the activated carbons AC 01 and AC 02 are shown in Figure S1 of the Supporting Information. It can be seen that the activated carbons have very low capacities for water in the concentration range investigated. Water probably adsorbs preferentially on active centers, such as oxygen functional groups, and this interaction favors the chemisorption of Hg^0. The oxygen functional groups and the water together form an active center for the chemisorption of elemental mercury. Physisorptive loading, on the other hand, does not benefit from high water partial pressures.

A comparison of the experiments with the washed activated carbons and the basic activated carbons shows that washing exposes or forms adsorption sites where mercury interacts chemisorptively with water from the gas phase. From the ultimate analyses (Table 5), it is evident that new oxygen functional groups are formed on the activated carbon AC 01 by oxidation of the surface during water washing. At the activated carbon AC 02, existing groups are presumably exposed that were previously blocked by mineral components.

To further investigate the mechanisms involved in chemisorption, coupled adsorption and desorption experiments were performed with CSA and TPD at different adsorption temperatures on the washed activated carbons. The plots of temperature-programmed desorption at adsorption temperatures of 30, 50, and 100 °C are shown in Figure 5. The washed activated carbons AC 01 (left) and AC 02 (right) were loaded with a mercury concentration of 264 $\mu g\ m^{-3}$ and a water partial pressure of 2.337 kPa.

The loadings and mass ratios of the coupled adsorption and desorption experiments are listed in Table 2.

Table 2. Mercury Loadings and Mass Ratios of the Coupled Adsorption and Desorption Experiments at Adsorption Temperatures of 30, 50, and 100 °C on the Washed Activated Carbons AC 01 and AC 02

		loading of Hg^0			
activated carbon	water partial pressure [kPa]	Ads. [$\mu g\ g^{-1}$]	CSA [$\mu g\ g^{-1}$]	TPD [$\mu g\ g^{-1}$]	mass ratio $\frac{x_{CSA}+x_{TPD}}{x_{Ads}}$
AC 01 washed	30	2.196	0.983	1.205	0.99
	50	1.364	0.536	0.769	0.95
	100	0.725	0.153	0.514	0.92
AC 02 washed	30	3.152	2.095	0.990	0.98
	50	2.191	1.428	0.583	0.92
	100	0.632	0.306	0.299	0.96

Figure 5 and Table 2 illustrate that by reducing the temperature from 100 to 30 °C, significantly more mercury is bound to the activated carbons physisorptively and chemisorptively. The ratio of desorbed to adsorbed mass is close to 1. Therefore, we suggest that mercury is completely desorbed in TPD as Hg^0. In the case of physisorption, more mercury is adsorbed at low temperatures, as expected. Due to the irreversible nature of chemisorption, the chemisorptive equilibrium state at moderate temperatures is always largely on the side of the products. According to the Arrhenius approach, the rate constant of chemical reactions increases with temperature because the activation energy can be overcome more easily. However, for the formation of a complex of water, mercury, and the activated carbon surface, physisorptive adsorption of the molecules is first necessary. The higher physisorptive loading of the activated carbon with water and Hg^0 at lower temperatures increases the probability that Hg^0 will be chemisorbed at an active site. This makes the kinetics of the reaction faster. Since more mercury is chemisorptively bound to the activated carbons at low temperatures, this effect seems to dominate over the deceleration of the reaction kinetics by lowering the rate constant. In contrast, Ambrosy et al.[37] found faster kinetics with increasing temperature in the case of chemisorption of Hg^0 with oxygen. This can be understood by assuming that the required activation energy for the chemisorption of mercury with water is lower than for the chemisorption of mercury with oxygen. It can be assumed that both reactions require dissociation of the coadsorptive, which is important for the value of the activation energy. Since the double bond between the oxygen atoms in the oxygen molecule is stronger than the single bond between the oxygen atom and the hydrogen atom in the water molecule, the dissociation energy of water is smaller than the dissociation energy of the oxygen molecule.

To examine whether the simultaneous presence of mercury and water in the gas phase is decisive for chemisorption, or whether adsorbed water modifies the activated carbon surface for chemisorption of mercury, simultaneous and sequential adsorption of mercury and water at 100 and at 30 °C were investigated.

Figure 6 shows the Hg^0 concentrations in TPD experiments with simultaneous adsorption of Hg^0 and water (black line) and sequential adsorption and desorption of water before adsorption of Hg^0 (green line) on washed activated carbons AC 01 (left) and AC 02 (right) at 100 °C. The experiments were performed with a water partial pressure of 2.337 kPa and a mercury concentration of 262 $\mu g\ m^{-3}$.

Table 3 provides the loadings and mass ratios for simultaneous and sequential adsorption.

When sequential adsorption and desorption of water occurs before the adsorption of Hg^0, the chemisorptive desorption peaks are very small (Figure 6) and only a small mass is desorbed (Table 3) compared to the simultaneous experiment. This demonstrates that significant chemisorption of Hg^0 requires both water and active sites on the activated carbon surface. Adsorption of water at 100 °C, followed by desorption at 100 °C is reversible and does not change the surface of the activated carbon. The ratio of desorbed to adsorbed mass is close to 1, so we can conclude that mercury desorption in TPD takes place completely in the form of Hg^0.

Figure 7 depicts the Hg^0 concentrations in TPD experiments with simultaneous adsorption of Hg^0 and water (black line), sequential adsorption and desorption of water before adsorption of Hg^0 (green line), and single-component adsorption of Hg^0 (blue line) on the washed activated carbons AC 01 (left) and AC 02 (right) at 30 °C.

The loadings and mass ratios of the experiments are shown in Table 4.

The amounts of Hg^0 desorbed by CSA (Table 4) show that coadsorption of water in the simultaneous experiment inhibits physisorption of mercury compared to the other experiments where no water is present in the gas phase during mercury adsorption. The ratio of desorbed to adsorbed mass is close to 1. This shows that the mercury desorbed in TPD is completely in the form of Hg^0.

https://doi.org/10.1021/acsomega.1c01994
ACS Omega 2021, 6, 16989−17001

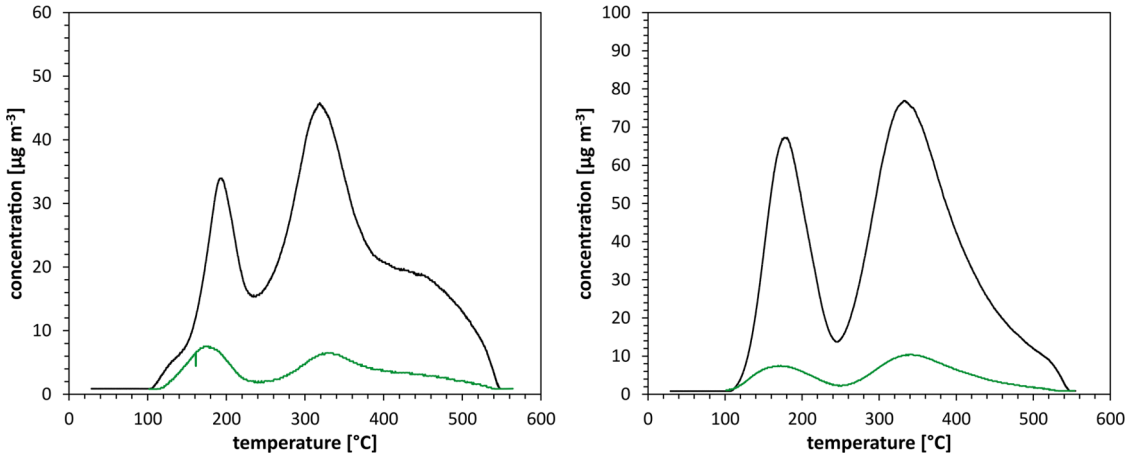

Figure 6. Hg^0 concentrations in TPD experiments with simultaneous adsorption of Hg^0 and water (black line) and sequential adsorption and desorption of water before adsorption of Hg^0 (green line) on washed activated carbons AC 01 (left) and AC 02 (right) at 100 °C and 2.337 kPa.

Table 3. Mercury Loadings and Mass Ratios for Simultaneous and Sequential Adsorption of Hg^0 and Water on Washed Activated Carbons AC 01 and AC 02 at 100 °C

		loading of Hg^0			
activated carbon	water partial pressure [kPa]	Ads. [$\mu g\ g^{-1}$]	CSA [$\mu g\ g^{-1}$]	TPD[$\mu g\ g^{-1}$]	mass ratio $\frac{X_{CSA}+X_{TPD}}{X_{Ads}}$
AC 01 washed	simultaneous	0.725	0.153	0.514	0.92
	sequential	0.337	0.241	0.078	0.94
AC 02 washed	simultaneous	1.149	0.239	1.005	1.08
	sequential	0.469	0.340	0.115	0.97

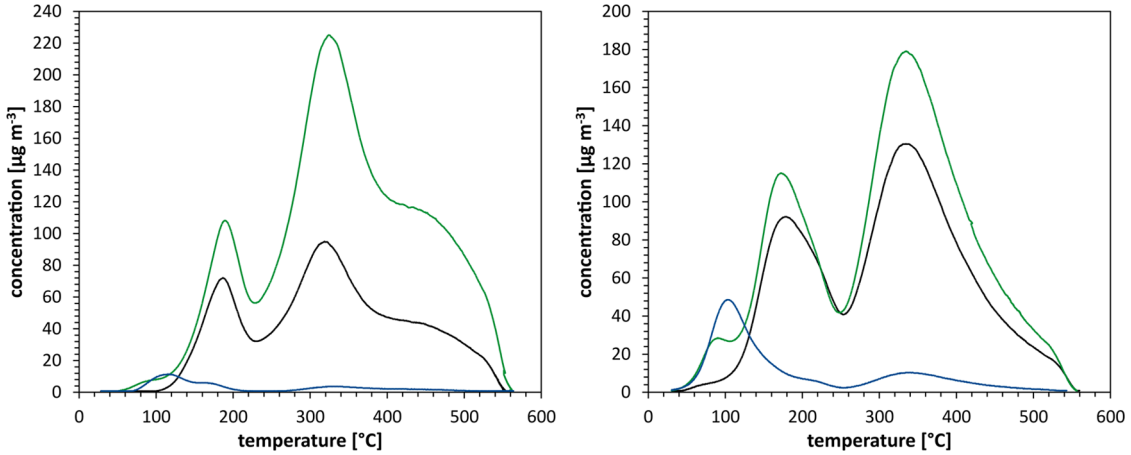

Figure 7. Hg^0 concentrations in TPD experiments with simultaneous adsorption of Hg^0 and water (black line), sequential adsorption and desorption of water before adsorption of Hg^0 (green line), and single-component adsorption of Hg^0 (blue line) on the washed activated carbons AC 01 (left) and AC 02 (right) at 30 °C.

Table 4. Mercury Loadings and Mass Ratios for Simultaneous and Sequential Adsorption of Hg^0 and Water and of Single-Component Adsorption of Hg^0 on Washed Activated Carbons AC 01 and AC 02 at 30 °C

		loading of Hg^0			
activated carbon	water partial pressure [kPa]	Ads. [$\mu g\ g^{-1}$]	CSA [$\mu g\ g^{-1}$]	TPD [$\mu g\ g^{-1}$]	mass ratio $\frac{X_{CSA}+X_{TPD}}{X_{Ads}}$
AC 01 washed	simultaneous	2.195	0.983	1.205	0.99
	sequential	4.778	1.859	2.778	0.97
	Hg^0 single-component	3.114	2.996	0.070	0.98
AC 02 washed	simultaneous	3.166	1.475	1.684	0.99
	sequential	4.930	2.594	2.306	0.99
	Hg^0 single-component	4.344	3.992	0.323	0.99

https://doi.org/10.1021/acsomega.1c01994
ACS Omega 2021, 6, 16989−17001

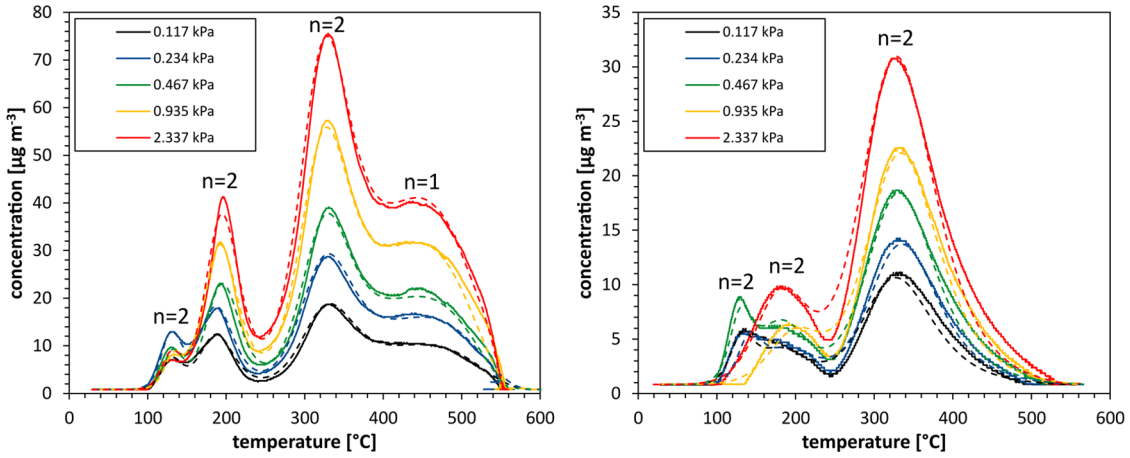

Figure 8. Experimental (solid line) and simulated (dashed line) Hg^0 concentrations of TPD experiments on washed activated carbons AC 01 (left) and AC 02 (right) with previous Hg^0 loading at 100 °C for 1 h and a water partial pressure range of 0.117−2.337 kPa.

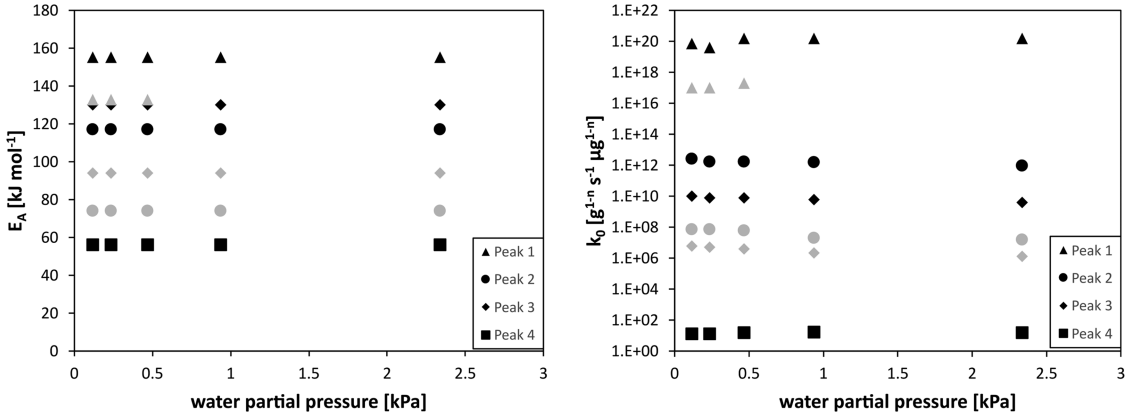

Figure 9. Activation energy of desorption E_A (left) and the frequency factor k_0 (right) of TPD experiments on washed activated carbons AC 01 (black) and AC 02 (gray) with previous Hg^0 loading at 100 °C for 1 h and a water partial pressure range of 0.117−2.337 kPa.

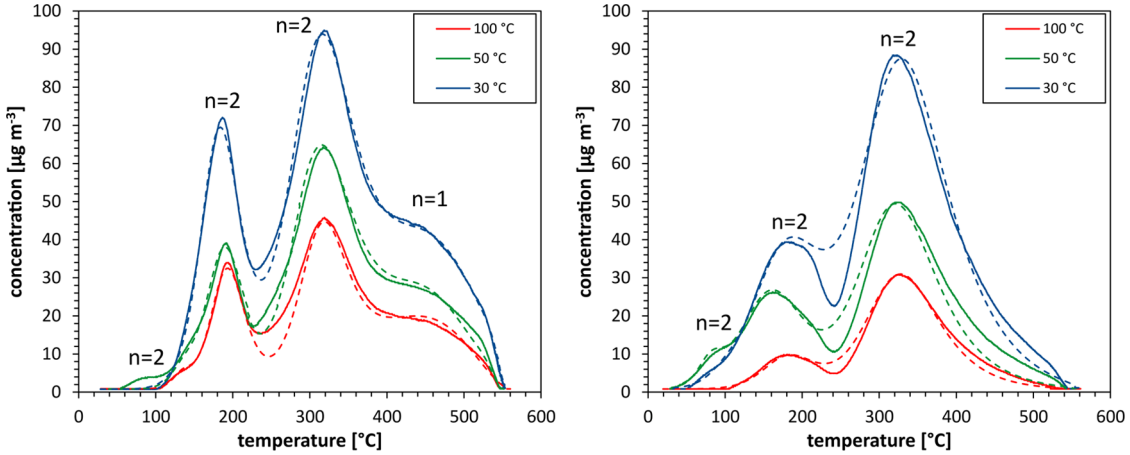

Figure 10. Experimental (solid line) and simulated (dashed line) concentrations of TPD experiments on washed activated carbons AC 01 (left) and AC 02 (right) with previous Hg^0 loading at 30−100 °C for 1 h and a water partial pressure of 2.337 kPa.

The concentration curves of the TPD experiments (Figure 7) indicate that in the experiments with sequential adsorption and desorption of water, a large part of the Hg^0 is chemisorptively bound. In contrast, fewer chemisorptive interactions are formed in simultaneous adsorption and almost none in single-component adsorption. Thus, as already observed for washing with water (Figure 1), the surface of the activated carbon is changed by the adsorption of water in the sequential experiment at 30 °C. In this respect, the result at 30 °C differs significantly from the result at 100 °C. It is possible that at the low desorption temperature, small amounts of water remain at the most energetically favorable adsorption sites, enhancing the chemisorption of Hg^0. Moreover, since no water is present in the gas phase during mercury adsorption in

https://doi.org/10.1021/acsomega.1c01994
ACS Omega 2021, 6, 16989−17001

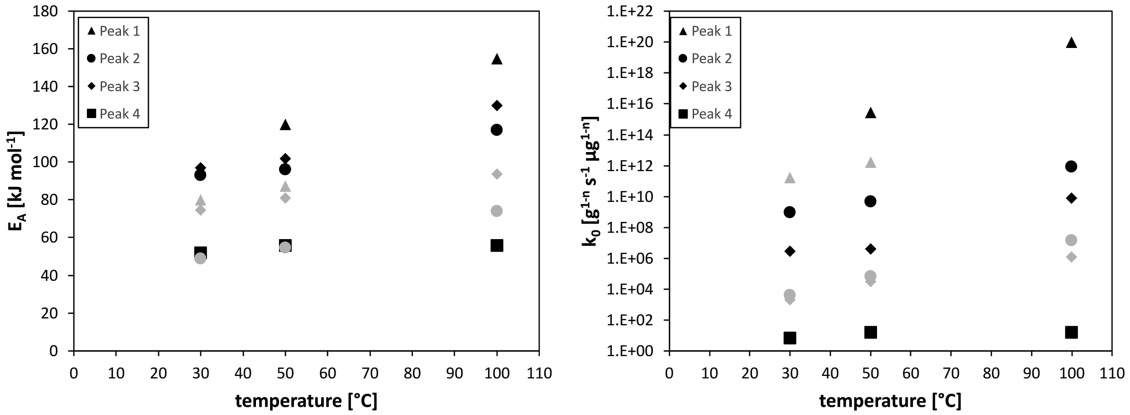

Figure 11. Activation energy of desorption E_A (left) and the frequency factor k_0 (right) for the TPD experiments on washed activated carbons AC 01 (black) and AC 02 (gray) with previous Hg^0 loading at 30−100 °C for 1 h and a water partial pressure of 2.337 kPa.

the sequential experiment at 30 °C, the physisorptive adsorption of mercury, which occurs before chemisorption, is not inhibited. For this reason, the strongest chemisorption of mercury is observed in the experiments with sequential adsorption and partial desorption of water at 30 °C. It is also clear from these experiments that for chemisorption of Hg^0, physisorbed water must be present on the surface. So, from our experiments it is obvious that several partners are involved in the chemisorption of mercury: physisorbed water, a functional oxygen group at the coal surface, and physisorbed mercury.

2.3. Kinetics of Hg^0 Desorption. The model presented in chapter 5 was used to represent the Hg^0 concentration profiles of the TPD experiments. The fit parameters E_A, k_0, and n were determined for each desorption peak. Figure 8 shows the experimental (solid line) and simulated (dashed line) concentrations of the TPD experiments on the washed activated carbons AC 01 (left) and AC 02 (right) with previous Hg^0 loading at 100 °C for 1 h and a water partial pressure range of 0.117−2.337 kPa. The determined reaction order is given in Figure 8 next to the desorption peaks. Figure 9 shows the fitted values of the activation energy of desorption E_A (left) and the frequency factor k_0 (right) of the individual desorption peaks.

The experimental data are well represented by the chemical−physical model. In the concentration range investigated, the activation energy and the frequency factor are independent of the loading.

Figure 10 presents the experimental (solid line) and simulated (dashed line) concentrations of the TPD experiments on the washed activated carbons AC 01 (left) and AC 02 (right) with previous Hg^0 loading at 30 to 100 °C for 1 h and a water partial pressure of 2.337 kPa. Figure 11 shows the values of the activation energy of desorption E_A (left) and the frequency factor k_0 (right) of the individual desorption peaks.

Both the frequency factor and the activation energy increase with increasing temperature. This dependence is typical for the frequency factor because the molecules become more mobile with increasing temperature. In heterogeneously catalyzed reactions, the reactants adsorb on the solid surface and in many cases form a transition state in which the bonds in the molecules of the reactants are weakened and new bonds begin to form in the molecules of the products. The adsorption step is less favorable at high temperatures due to the increased mobility of the molecules. As a result, there can be a distortion of the transition state, which is then also less favorable energetically. This effect leads to an activation energy that increases with temperature. This behavior is expected for heterogeneously catalyzed reactions in which a transition state at an active site on the surface controls the activation energy.

3. CONCLUSIONS

The influence of water on physisorption and chemisorption of mercury was investigated using breakthrough and TPD experiments. Basic and washed materials were compared. Little influence of water was found on mercury adsorption on the basic materials. It was shown that washing the activated carbons with water increases the number of exposed oxygen functional groups on the surface of the activated carbons AC 01 and AC 02. For significant chemisorption of mercury with these groups, adsorbed water must be present on the activated carbon. This reveals that for effective chemisorption of mercury, oxygen functional groups are needed along with water on the surface.

However, the physisorptive accumulation of mercury that precedes chemisorption is inhibited by the coadsorption of water. So, the highest chemisorption rates were found in the case of sequential adsorption and partial desorption of water at 30 °C. Here, water changes the surface chemistry without inhibiting mercury physisorption.

Chemisorption is better at 30 °C than at 100 °C. The effect of higher physisorptive loading at lower temperature prevails over the effect of the smaller reaction rate constant.

The detection of several desorption peaks at different desorption temperatures suggests different chemisorptive mechanisms with mercury, water, and different oxygen functional groups. Simulation with a transport model extended by an approach for chemisorption was used to determine reaction parameters (activation energy, frequency factor, and reaction order) for each desorption mechanism. The activation energy and the frequency factor increase with temperature and are independent of the loading in the concentration range investigated. This is typical for heterogeneously catalyzed reactions where the activation energy is dominated by a transition state at an active site on the surface.

In subsequent works, the complex process of mercury chemisorption on activated carbons should be further investigated. For this purpose, the number of heteroatoms on the surface of the activated carbon could be systematically varied by oxidizing and reducing treatments. These materials

https://doi.org/10.1021/acsomega.1c01994
ACS Omega 2021, 6, 16989−17001

Table 5. Chemical Composition of the Adsorbents

			[weight % of dry mass]					
activated carbon	raw material	activation method	ash content	C	S	N	H	O
AC 01	anthracite	steam	10.7	87.4	0.24	0.32	0.53	0.8
AC 01 washed	anthracite	steam	5.7	85.2	0.10	0.19	0.74	5.4
AC 02	coconut shell	steam	2.9	90.4	0.44	0.23	0.51	5.5
AC 02 washed	coconut shell	steam	<0.1	94.9	<0.10	0.25	0.54	4.3

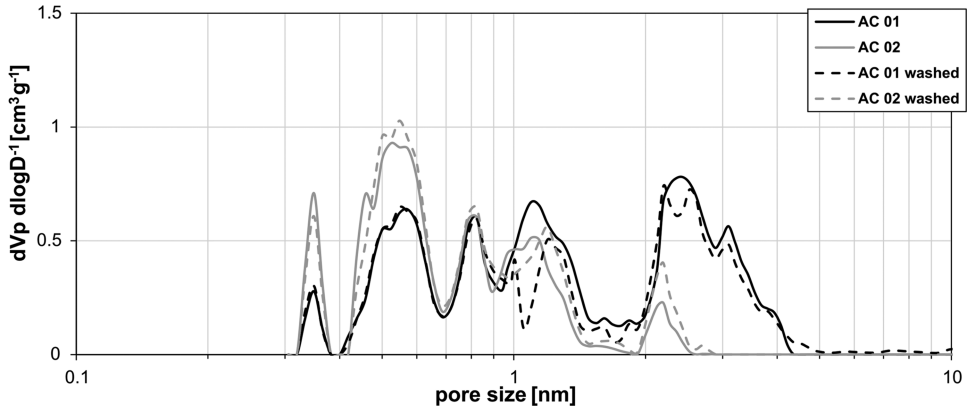

Figure 12. Pore size distribution of AC 01 and AC 02.

Table 6. Structural Properties of the Used Activated Carbons

property	AC 01	AC 01 washed	AC 02	AC 02 washed
BET-surface [$m^2 \cdot g^{-1}$]	1079	1025	951	945
total pore volume [$cm^3 \cdot g^{-1}$]	0.494	0.482	0.391	0.390
micropore volume [$cm^3 \cdot g^{-1}$]	0.387	0.382	0.376	0.387

should first be characterized in detail by various measurement methods such as nitrogen isotherms, Boehm titration, X-ray photoelectron spectroscopy (XPS), or infrared spectroscopy (IR). The basic and modified materials can then be used to study mercury adsorption and desorption.

4. MATERIALS

Two commercial activated carbons AC 01 and AC 02 (delivered by Carbon Service & Consulting GmbH & Co. KG) of granular form with a particle size range of 1.6−2 mm were used as basic materials. Activated carbon AC 01 was based on anthracite and AC 02 on coconut shells, and both were activated with steam. The activated carbons were modified by a water wash with deionized water at 90 °C for 20 min followed by elution steps to remove the dissolved ash components at 30 °C. The wash process was terminated when the supernatant eluate had a conductivity of <30 μS cm^{-1} after a shaking time of 10 h. Table 5 summarizes the relevant data on the material properties for adsorption of the basic and washed materials.

The adsorbents consist mainly of carbon with small quantities of sulfur, nitrogen, and hydrogen. The wash reduces the ash content of both activated carbons. The higher oxygen content of the washed AC 01 is due to oxidation of the surface, which probably increases the number of functional oxygen groups. This effect is not clearly understood yet. Maybe water reacts with defects in the graphitic regions of the carbon matrix, thus creating new oxygen functional groups on the surface of the activated carbon. Nevertheless, the increase in oxygen content is surprising. For this reason, reproducibility measurements of the elemental analyses were made, which confirmed the results. The oxygen content of the AC 02 is not increased by the wash.

The adsorptive Hg^0 is fed to the adsorber using a nitrogen stream with a purity of 99.9999% and a dew point of <−80 °C as the carrier gas. Some thermodynamic data of the adsorptive Hg^0 are displayed in Table S1 in the Supporting Information.

4.1. Conditioning and Volumetric Characterization of Adsorbents. Nitrogen isotherms at 77 K and carbon dioxide isotherms at 273 K were measured using a volumetric measurement device (Belsorp-max from Bel Japan, Inc.) to characterize the adsorbents.[46] The samples were prepared at 175 °C under vacuum (<10^{-3} Pa) for 6 h. The pore size distribution (Figure 12) was defined by quenched solid density functional theory (QSDFT) with a slit and cylindrical pore model.[47] The specific surface area was calculated using the Brunauer−Emmett−Teller (BET) method according to DIN ISO 9277. The micropore volume was determined according to DIN 66135 using the Dubinin−Radushkevich method.[48] Table 6 shows the structural properties of the adsorbents. The nitrogen isotherms are displayed in Figure S2 of the Supporting Information.

The calculated structural properties and the pore size distribution reveal that the modifications have no significant influence on the pore structure of the activated carbons.

4.2. Experimental Approach. The experimental plant used for adsorption and desorption experiments is presented in Figure 13 and has already been described in detail in an earlier publication.[31] In the gas mixing unit, a defined mixture of Hg^0, nitrogen, and water (0−2.337 kPa) is provided by mass flow controllers (MFC). The highest adjustable water partial

https://doi.org/10.1021/acsomega.1c01994
ACS Omega 2021, 6, 16989−17001

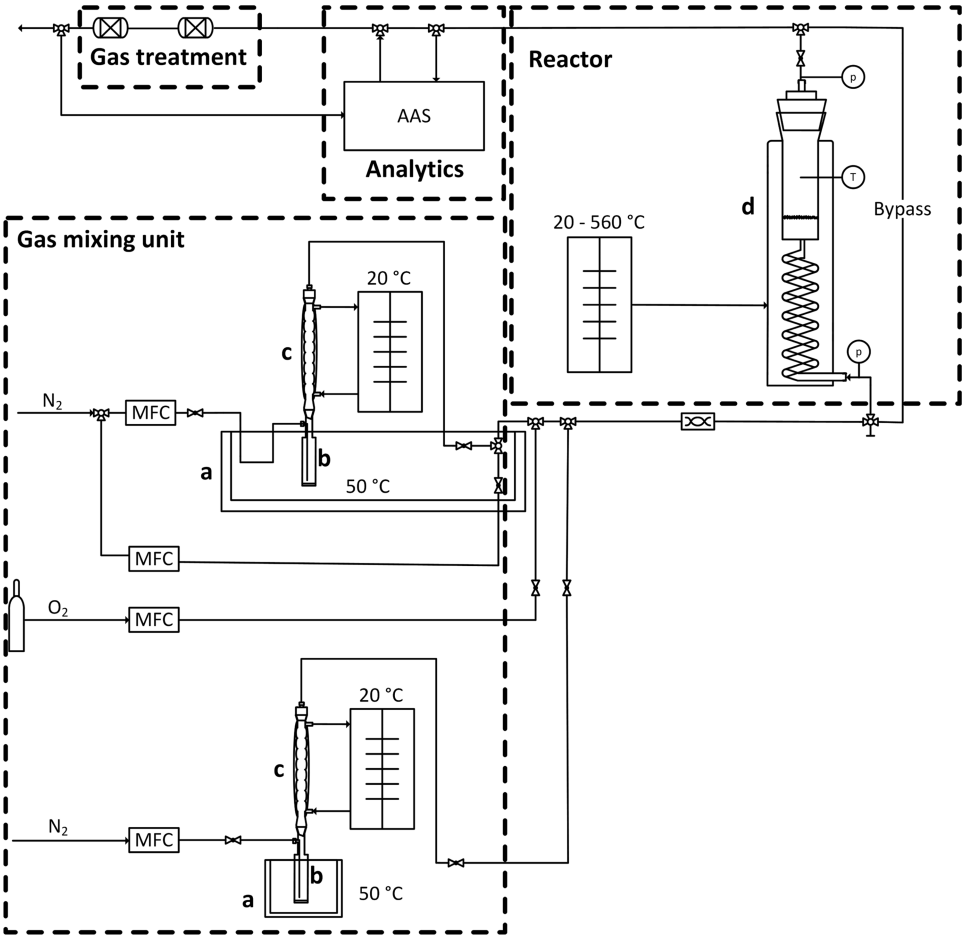

Figure 13. Flow sheet of the fixed bed test unit; a = water bath; b = evaporator; c = cooler; d = tempered reactor; MFC = mass flow controller; and AAS = atomic absorption spectrometer.

pressure is the saturation vapor pressure at 20 °C. To avoid condensation in the pipes, the temperature in the laboratory is above 20 °C. Adsorption takes place in a glass vessel, in which the fed gas and the fixed bed of activated carbon are tempered by a heating jacket in the range of 20−560 °C. The mercury concentration is continuously detected by an atomic absorption spectrometer VM 3000 of Mercury Instruments GmbH. The exhaust gas is purified by two chemisorptive adsorbers filled with sulfur-impregnated activated carbon.

The activated carbons are conditioned as mentioned above before the start of the experiments. Then, they are filled into the reactor and flushed with nitrogen. After reaching the adsorption temperature, mercury and water are dosed into the gas phase through the bypass with the reactor closed. If a constant concentration is measured over a period of 20 min, the experiment begins by redirecting the gas stream to the fixed bed. To investigate the chemisorption of Hg^0, coupled adsorption and desorption experiments with temperature-programmed desorption were performed. The experiments can be divided into three sections: adsorption, concentration swing desorption (CSA), and temperature-programmed desorption (TPD). In the adsorption part of the experiment, the mercury-containing nitrogen stream is passed over the fixed bed at constant temperature for a defined time of 1 h. The mercury loading of the adsorbent can be calculated by integrating the area above the measured breakthrough curve. Assuming that only mercury is adsorbed and that the density of the gas at the inlet of the fixed adsorbent bed is equal to the density at the outlet of the bed, the global mass balance around the adsorbent bed yields

$$X = \frac{m_{\mathrm{Hg,Ads}}}{m_{\mathrm{s}}} = \frac{\dot{V}_{\mathrm{ges}}}{m_{\mathrm{s}}} \cdot \sum_{t=0}^{t=T} \left(\frac{c_{\mathrm{Hg,in}} - c_{\mathrm{Hg,out}}}{\left(1 - \frac{c_{\mathrm{Hg,out}}}{\rho_{\mathrm{G}}}\right)} \right) \cdot \Delta t_i \quad (1)$$

Here, $m_{\mathrm{Hg,Ads}}$ is the mass of the adsorptive, m_{s} is the mass of the adsorbent, and $\dot{V}_{\mathrm{ges}}$ is the volume flow of the gas.

During the adsorption part, oxygen or water can be additionally dosed into the gas phase. In the further steps (CSA and TPD), the activated carbons are purged with pure nitrogen. After the adsorbent has been loaded for 1 h, a concentration swing desorption follows, by which the physisorptively bound mercury is desorbed. For this purpose, the adsorber is flushed with pure nitrogen at the same temperature where adsorption took place, until no more mercury is detected. Then, the temperature-programmed desorption begins, which desorbs the chemisorptively bound mercury. The temperature is continuously increased in a ramp function of 5 °C min^{-1} up to 560 °C. The desorbed mass of mercury during concentration swing desorption (X_{CSA}) and temperature-programmed desorption (X_{TPD}) is calculated by eq 1. The input concentration $c_{\mathrm{Hg,in}}$ corresponds to the zero line of the measuring device. The mass ratio of adsorption and desorption (CSA and TPD) can be calculated using eq 2

https://doi.org/10.1021/acsomega.1c01994
ACS Omega 2021, 6, 16989−17001

$$\text{mass ratio} = \frac{X_{CSA} + X_{TPD}}{X_{Ads}} \cdot 100\% \quad (2)$$

5. COMPUTATIONAL METHODS

Modeling of TPD experiments was performed with a transport model extended by an approach for chemisorption. The aim was to simulate the concentration and temperature profiles to obtain information about the chemical desorption reactions taking place. For this purpose, the adsorber is divided into n equal increments of height dz. For each increment, three energy balances and two mass balances are established. The partial differential equation system is solved iteratively using an Euler finite difference method. The following assumptions are made:

- Ideal gas behavior of the fluid phase.
- Carrier gas is inert.
- Uniform diameter of spherical adsorbent particles.
- Radial gradients of the concentration and temperature are neglected.
- Pressure drop in the fixed bed is neglected.
- Axial dispersion is calculated according to the approach of Wakao.[49]
- Reaction kinetics is slow compared to diffusion processes.
- Adsorption enthalpy is neglected in the energy balance due to small loadings.
- Readsorption of mercury is neglected.
- Mercury compounds formed by chemisorption decompose to Hg^0.

With these assumptions the mass balance of the fluid phase (eq 3) yields[50,51]

$$\frac{\partial c}{\partial t} = D_{ax}\frac{\partial^2 c}{\partial z^2} - \frac{\dot{V}_G}{A\cdot\varepsilon_L}\frac{\partial c}{\partial z} - \frac{c}{A\cdot\varepsilon_L}\frac{\partial \dot{V}_G}{\partial z} - \rho_s\frac{(1-\varepsilon_L)}{\varepsilon_L}\frac{\partial X}{\partial t} \quad (3)$$

The parameter c is the mercury concentration in the gas phase, D_{ax} is the axial dispersion coefficient, A is the column cross section, ε_L is the bed porosity, and ρ_s is the apparent density of an adsorbent particle.

The Polanyi−Wigner equation is predominantly used in the literature for evaluating TPD experiments on single grains or smaller sample quantities.[52] It describes the thermal desorption kinetics by means of a simple potential function. Due to the very slow reaction kinetics and very high capacities of some activated carbons for Hg^0, it is often not possible to measure the equilibrium, therefore the monomolecular loading cannot be determined. This is why the loading X is used instead of the degree of coverage to describe the desorption rate. The temperature is related to time by the heating rate $\frac{dT_G}{dt} = \beta$. In analogy to the rate law of chemical reactions, the following equation results.

$$r(X) = \frac{\partial X}{\partial t} = k_0\cdot\exp\left[-\frac{E_A}{R\cdot T_G}\right]\cdot X^n \quad (4)$$

The activation energy E_A, the reaction order n, and the pre-exponential factor k_0 are fitted to experimentally measured curves.

If the desorption consists of several mechanisms, the mass balance of the solid phase is composed of the corresponding number of terms

$$\frac{\partial X}{\partial t} = \frac{\partial X_1}{\partial t} + \frac{\partial X_2}{\partial t} + \ldots + \frac{\partial X_i}{\partial t} \quad (5)$$

Each term is described by eq 4 and represents a desorption mechanism.

For the dynamic simulation of the heat transport in the adsorber, an energy balance of the solid phase (eq 6) and the fluid phase (eq 7) is used. The energy balance of the solid phase S includes the heat released during adsorption, the heat stored in the packing, and the heat transfer between the gas phase and the solid phase. In the energy balance of the fluid phase G, the energy exchange between the fluid and solid phases, the transport terms of convection and dispersion, the storage terms of the gas phase, and the heat transport through the adsorber wall are considered.[30,37]

$$\frac{\partial T_S}{\partial t} = \frac{-\alpha_p\cdot A_{sp}}{\rho_S\cdot(c_{p,S} + X\cdot c_{p,A})}\cdot(T_S - T_G) + \frac{\Delta h_{Ads}}{M_A\cdot(c_{p,S} + X\cdot c_{p,A})}\cdot\frac{\partial X}{\partial t} \quad (6)$$

$$\frac{\partial T_G}{\partial t} = -\frac{\partial \dot{V}_G}{\partial z}\cdot\frac{T_G}{A\cdot\varepsilon_L} - \frac{\partial \rho_G}{\partial z}\cdot\frac{\dot{V}_G\cdot T_G}{A\cdot\varepsilon_L\cdot\rho_G} - \frac{\partial T_G}{\partial z}\cdot\frac{\dot{V}_G}{A\cdot\varepsilon_L} + \frac{\lambda_D}{\rho_G\cdot c_{p,G}}\cdot\frac{\partial^2 T_G}{\partial(z)^2} + \frac{\alpha_p\cdot(1-\varepsilon_L)\cdot A_{sp}}{\rho_G\cdot c_{p,G}\cdot\varepsilon_L}(T_S - T_G) - \frac{\rho_S\cdot(1-\varepsilon_L)\cdot c_{p,A}}{\rho_G\cdot c_{p,G}\cdot\varepsilon_L}(T_S + T_G)\frac{\partial X}{\partial t} - \frac{\alpha_{w,i}}{d_i\cdot\rho_G\cdot c_{p,G}\cdot\varepsilon_L}(T_G - T_W) \quad (7)$$

The quantities α_p and $\alpha_{w,i}$ represent the heat transfer coefficients from the fluid to the solid phase and from the gas phase to the adsorber inner wall. The parameters $c_{p,s}$, $c_{p,A}$, and $c_{p,G}$ describe the specific heat capacities of the adsorbent, the adsorptive, and the gas phase. The quantity d_i is the inside diameter of the adsorber. Furthermore, the density of the gas phase ρ_G and the disperse thermal conductivity coefficient λ_D are used.

The initial and boundary conditions required for the solution of the differential equation system, as well as the auxiliary equations and quantities, are described in the Supporting Information.

■ ASSOCIATED CONTENT

Supporting Information

The Supporting Information is available free of charge at https://pubs.acs.org/doi/10.1021/acsomega.1c01994.

Additional equations and quantities used for modeling physical properties of Hg^0; water isotherms; and nitrogen isotherms (PDF)

■ AUTHOR INFORMATION

Corresponding Author

Julian Steinhaus − *Chair of Thermal Process Engineering, University of Duisburg-Essen, D-47057 Duisburg, Germany;* orcid.org/0000-0002-5621-8186; Email: julian.steinhaus@uni-due.de

https://doi.org/10.1021/acsomega.1c01994
ACS Omega 2021, 6, 16989−17001

Authors

Christoph Pasel − *Chair of Thermal Process Engineering, University of Duisburg-Essen, D-47057 Duisburg, Germany*

Christian Bläker − *Chair of Thermal Process Engineering, University of Duisburg-Essen, D-47057 Duisburg, Germany*

Dieter Bathen − *Chair of Thermal Process Engineering, University of Duisburg-Essen, D-47057 Duisburg, Germany; Institute of Energy and Environmental Technology, IUTA e. V., D-47229 Duisburg, Germany*

Complete contact information is available at: https://pubs.acs.org/10.1021/acsomega.1c01994

Notes

The authors declare no competing financial interest.

■ ACKNOWLEDGMENTS

The work is funded by Deutsche Forschungsgemeinschaft (DFG), project BA 2012/14-1. We acknowledge support by the Open Access Publication Fund of the University of Duisburg-Essen. The activated carbons are kindly provided by Carbon Service & Consulting GmbH & Co KG.

■ NOMENCLATURE

A	cross-sectional area of the adsorber column, m^2
A_{sp}	specific area of the particle, $m^2 \cdot m^{-3}$
c	concentration of mercury in the gas phase, $\mu g \cdot m^{-3}$
$c_{p,A}$	specific heat capacity of the adsorptive, $J \cdot kg^{-1} \cdot K^{-1}$
$c_{p,G}$	Specific heat capacity of the gas phase, $J \cdot kg^{-1} \cdot K^{-1}$
$c_{p,s}$	Specific heat capacity of the adsorbent, $J \cdot kg^{-1} \cdot K^{-1}$
d_i	diameter of the adsorber, m
d_a	outer diameter of the adsorber, m
D_{ax}	axial dispersion coefficient, $m^2 \cdot s^{-1}$
D_{12}	effective homogeneous diffusion coefficient, $m^2 \cdot s^{-1}$
E_A	activation energy of the chemical reaction, $J \cdot mol^{-1}$
k_0	pre-exponential factor, $g^n\ \mu g^{-n}\ s^{-1}$
L	length of the adsorber, m
M_A	molar mass of adsorptive, $g \cdot mol^{-1}$
n	reaction order
t	time, s
T_G	temperature of the gas phase, K
T_S	temperature of the solid phase, K
T_A	ambient temperature, K
T_W	temperature of the adsorber wall, K
$\dot{V}_G$	volume flow of the gas stream, $l_n \bullet min^{-1}$
X	loading, $\mu g \cdot g^{-1}$
α_p	heat transfer coefficient between the fluid and solid phase, $W \cdot m^{-2} \cdot K^{-1}$
$\alpha_{w,i}$	heat transfer coefficient between the fluid phase and adsorber wall, $W \cdot m^{-2} \cdot K^{-1}$
$\alpha_{w,a}$	heat transfer coefficient between the adsorber wall and environment, $W \cdot m^{-2} \cdot K^{-1}$
β_{Film}	film transport coefficient, $m^2 \cdot s^{-1}$
Δh_{Ads}	heat of adsorption, $J \cdot mol^{-1}$
ε_L	bed porosity
ε_p	particle porosity
λ_D	axial dispersion coefficient of thermal conductivity, $W \cdot m^{-1} \cdot K^{-1}$
ρ_G	gas density, $kg \cdot m^{-3}$
ρ_p	average density of the particle, $kg \cdot m^{-3}$
ρ_s	apparent density of the particle, $kg \cdot m^{-3}$
ρ_w	density of the adsorber wall, $kg \cdot m^{-3}$

■ REFERENCES

(1) Serre, S. D.; Gullett, B. K.; Ghorishi, S. B. Entrained-flow adsorption of mercury using activated carbon. *J. Air Waste Manage. Assoc.* **2001**, *51*, 733−741.

(2) Chen, Y.; Liu, H.; Guo, X.; Wu, F.; Zhao, Y.; Zhang, J. Performance of $CuCl_2$-Modified Activated Carbon on Mercury Capture after Injection in an Entrained Flow Reactor. *Ind. Eng. Chem. Res.* **2020**, *59*, 5557−5565.

(3) Liu, H.; Chen, Y.; Gao, T.; Yang, G.; Wang, Y.; Zhou, Y.; Yang, J.; Zhao, Y.; Guo, X.; Zhang, J. Elemental mercury removal from flue gas using modified tonstein: Performance of adsorbent injection at an entrained flow reactor system and 50-MW coal-fired power plant in China. *J. Cleaner Prod.* **2021**, *287*, No. 124998.

(4) *Emission Control-Human Cremation Facilities*; VDI 3891, Beuth Verlag, Berlin, 2015.

(5) Xu, J.; Bao, J.; Tang, J.; Du, M.; Liu, H.; Xie, G.; Yang, H. Characteristics and Inhibition of Hg^0 Re-emission in a Wet Flue Gas Desulfurization System. *Energy Fuels* **2018**, *32*, 6111−6118.

(6) Li, Z.; Chen, X.; Liu, W.; Li, T.; Chen, J.; Lin, C.-J.; Sun, G.; Feng, X. Evolution of four-decade atmospheric mercury release from a coal-fired power plant in North China. *Atmos. Environ.* **2019**, *213*, 526−533.

(7) Hsi, H.-C.; Rood, M. J.; Rostam-Abadi, M.; Chen, S.; Chang, R. Mercury Adsorption Properties of Sulfur-Impregnated Adsorbents. *J. Environ. Eng.* **2002**, *128*, 1080−1089.

(8) Hsi, H.-C.; Tsai, C.-Y.; Lin, K.-J. Impact of Surface Functional Groups, Water Vapor, and Flue Gas Components on Mercury Adsorption and Oxidation by Sulfur-Impregnated Activated Carbons. *Energy Fuels* **2014**, *28*, 3300−3309.

(9) Liu, W.; Vidic, R. D.; Brown, T. D. Optimization of High Temperature Sulfur Impregnation on Activated Carbon for Permanent Sequestration of Elemental Mercury Vapors. *Environ. Sci. Technol.* **2000**, *34*, 483−488.

(10) Lee, S. J.; Seo, Y.-C.; Jurng, J.; Lee, T. G. Removal of gas-phase elemental mercury by iodine- and chlorine-impregnated activated carbons. *Atmos. Environ.* **2004**, *38*, 4887−4893.

(11) Sinha, R. K.; Walker, P. L. Removal of Mercury by Sulfurized Carbons. *Carbon* **1972**, *10*, 754−756.

(12) Tan, Z.; Qiu, J.; Zeng, H.; Liu, H.; Xiang, J. Removal of elemental mercury by bamboo charcoal impregnated with H_2O_2. *Fuel* **2011**, *90*, 1471−1475.

(13) Tan, Z.; Sun, L.; Xiang, J.; Zeng, H.; Liu, Z.; Hu, S.; Qiu, J. Gas-phase elemental mercury removal by novel carbon-based sorbents. *Carbon* **2012**, *50*, 362−371.

(14) Hsi, H.-C.; Chen, C.-T. Influences of acidic/oxidizing gases on elemental mercury adsorption equilibrium and kinetics of sulfur-impregnated activated carbon. *Fuel* **2012**, *98*, 229−235.

(15) Hsi, H.-C.; Rood, M. J.; Rostam-Abadi, M.; Chen, S.; Chang, R. Effects of Sulfur Impregnation Temperature on the Properties and Mercury Adsorption Capacities of Activated Carbon Fibers (ACFs). *Environ. Sci. Technol.* **2001**, *35*, 2785−2791.

(16) Otani, Y.; Kanaoka, C.; Emi, H.; Uchijima, I.; Nishino, H. Removal of mercury vapor from air with sulfur-impregnated adsorbents. *Environ. Sci. Technol.* **1988**, *22*, 708−711.

(17) Olson, E. S.; Miller, S. J.; Sharma, R. K.; Dunham, G. E.; Benson, S. A. Catalytic effects of carbon sorbents for mercury capture. *J. Hazard. Mater.* **2000**, *74*, 61−79.

(18) Diamantopoulou, I.; Skodras, G.; Sakellaropoulos, G. P. Sorption of mercury by activated carbon in the presence of flue gas components. *Fuel Process. Technol.* **2010**, *91*, 158−163.

(19) Korpiel, J. A.; Vidic, R. D. Effect of Sulfur Impregnation Method on Activated Carbon Uptake of Gas-Phase Mercury. *Environ. Sci. Technol.* **1997**, *31*, 2319−2325.

(20) Krishnan, S. V.; Gullett, B. K.; Jozewicz, W. Mercury control in municipal waste combustors and coal-fired utilities. *Environ. Prog.* **1997**, *16*, 47−53.

(21) Krishnan, S. V.; Gullett, B. K.; Jozewicz, W. Sorption of Elemental Mercury by Activated Carbons. *Environ. Sci. Technol.* **1994**, *28*, 1506−1512.

(22) Skodras, G.; Diamantopoulou, I.; Zabaniotou, A.; Stavropoulos, G.; Sakellaropoulos, G. P. Enhanced mercury adsorption in activated carbons from biomass materials and waste tires. *Fuel Process. Technol.* **2007**, *88*, 749−758.
(23) Skodras, G.; Diamantopoulou, I.; Sakellaropoulos, G. P. Role of activated carbon structural properties and surface chemistry in mercury adsorption. *Desalination* **2007**, *210*, 281−286.
(24) Skodras, G.; Diamantopoulou, I.; Pantoleontos, G.; Sakellaropoulos, G. P. Kinetic studies of elemental mercury adsorption in activated carbon fixed bed reactor. *J. Hazard. Mater.* **2008**, *158*, 1−13.
(25) Musmarra, D.; Karatza, D.; Lancia, A.; Prisciandaro, M.; Mazziotti, G.; Di Mazziotti Celso, G. A Comparison among Different Sorbents for Mercury Adsorption from Flue Gas. *Chem. Eng. Trans* **2015**, *43*, 2461−2466.
(26) Liu, J.; Cheney, M. A.; Wu, F.; Li, M. Effects of chemical functional groups on elemental mercury adsorption on carbonaceous surfaces. *J. Hazard. Mater.* **2011**, *186*, 108−113.
(27) Karatza, D.; Prisciandaro, M.; Lancia, A.; Musmarra, D. Silver impregnated carbon for adsorption and desorption of elemental mercury vapors. *J. Environ. Sci.* **2011**, *23*, 1578−1584.
(28) Karatza, D.; Lancia, A.; Prisciandaro, M.; Musmarra, D.; Di Mazziotti Celso, G. Influence of oxygen on adsorption of elemental mercury vapors onto activated carbon. *Fuel* **2013**, *111*, 485−491.
(29) Ho, T. C.; Kobayashi, N.; Lee, Y. K.; Lin, C. J.; Hopper, J. R. Modeling of mercury sorption by activated carbon in a confined, a semi-fluidized, and a fluidized bed. *Waste Manage.* **2002**, *22*, 391−398.
(30) Ambrosy, J. M.; Steinhaus, J.; Pasel, C.; Bläker, C.; Bittig, M.; Bathen, D. Simulative Investigation of the Application of Non-impregnated Activated Carbon in a Multilayer Adsorber for the Separation of Hg^0 from Discontinuous Waste Gas Streams. *Ind. Eng. Chem. Res.* **2021**, *60*, 4097−4109.
(31) Ambrosy, J. M.; Pasel, C.; Luckas, M.; Bittig, M.; Bathen, D. A Detailed Investigation of Adsorption Isotherms, Enthalpies, and Kinetics of Mercury Adsorption on Nonimpregnated Activated Carbon. *Ind. Eng. Chem. Res.* **2019**, *58*, 4208−4221.
(32) Ambrosy, J. M.; Pasel, C.; Luckas, M.; Bittig, M.; Bathen, D. Comprehensive Methodology for the Investigation of Mercury Adsorption on Activated Carbons. *Chem. Ing. Tech.* **2019**, *91*, 1874−1884.
(33) Li, Y. H.; Lee, C. W.; Gullett, B. K. The effect of activated carbon surface moisture on low temperature mercury adsorption. *Carbon* **2002**, *40*, 65−72.
(34) Hall, B.; Schager, P.; Weesmaa, J. The homogeneous gas phase reaction of mercury with oxygen, and the corresponding heterogeneous reactions in the presence of activated carbon and fly ash. *Chemosphere* **1995**, *30*, 611−627.
(35) Sun, P.; Zhang, B.; Zeng, X.; Luo, G.; Li, X.; Yao, H.; Zheng, C. Deep study on effects of activated carbon's oxygen functional groups for elemental mercury adsorption using temperature programmed desorption method. *Fuel* **2017**, *200*, 100−106.
(36) Zeng, H.; Jin, F.; Guo, J. Removal of elemental mercury from coal combustion flue gas by chloride-impregnated activated carbon. *Fuel* **2004**, *83*, 143−146.
(37) Ambrosy, J. M.; Pasel, C.; Luckas, M.; Bittig, M.; Bathen, D. Influence of Oxygen on Hg^0 Adsorption on Non-Impregnated Activated Carbons. *ACS omega* **2020**, *5*, 17051−17061. Published Online: Jul. 8, 2020
(38) Yan, R.; Ng, Y. L.; Liang, D. T.; Lim, C. S.; Tay, J. H. Bench-Scale Experimental Study on the Effect of Flue Gas Composition on Mercury Removal by Activated Carbon Adsorption. *Energy Fuels* **2003**, *17*, 1528−1535.
(39) Liu, W.; Vidic, R. D.; Brown, T. D. Impact of Flue Gas Conditions on Mercury Uptake by Sulfur-Impregnated Activated Carbon. *Environ. Sci. Technol.* **2000**, *34*, 154−159.
(40) Lopez-Anton, M. A.; Ferrera-Lorenzo, N.; Fuente, E.; Díaz-Somoano, M.; Suarez-Ruíz, I.; Martínez-Tarazona, M. R.; Ruiz, B. Impact of oxy-fuel combustion gases on mercury retention in activated carbons from a macroalgae waste: effect of water. *Chemosphere* **2015**, *125*, 191−197.
(41) Lopez-Anton, M. A.; Rumayor, M.; Díaz-Somoano, M.; Martínez-Tarazona, M. R. Influence of a CO2-enriched flue gas on mercury capture by activated carbons. *Chem. Eng. J.* **2015**, *262*, 1237−1243.
(42) Rafeen, S.; Ramli, R.; Srinivasan, G. Tackling elemental mercury removal from the wet-gas phase by enhancing the performance of redox-active copper-based adsorbents utilising an operando pre-heating system. *React. Chem. Eng.* **2020**, *5*, 1647.
(43) Hsi, H.-C.; Tsai, C. Y.; Lin, K. J. Impact of Surface Functional Groups, Water Vapor, and Flue Gas Components on Mercury Adsorption and Oxidation by Sulfur-Impregnated Activated Carbons. *Energy Fuels* **2014**, *28*, 3300−3309.
(44) Hu, C.; Hang, D.; Guo, R.; Guo, Z.; Yu, X. Influence of H_2O on Hg^0 Oxidation in the Simulated Flue Gas in Oxygen-Enriched Combustion. *Energy Fuels* **2017**, *31*, 7272−7281.
(45) Wang, H.; Shen, C.; Duan, Y.; Ying, Z.; Li, Y. N. Synergistic effect between H_2O and SO_2 on mercury removal by activated carbon in O_2/CO_2 conditions. *J. Chem. Technol. Biotechnol.* **2019**, *94*, 1195−1201.
(46) Bläker, C.; Muthmann, J.; Pasel, C.; Bathen, D. Characterization of Activated Carbon Adsorbents − State of the Art and Novel Approaches. *ChemBioEng Rev.* **2019**, *6*, 119−138.
(47) Neimark, A. V.; Lin, Y.; Ravikovitch, P. I.; Thommes, M. Quenched solid density functional theory and pore size analysis of micro-mesoporous carbons. *Carbon* **2009**, *47*, 1617−1628.
(48) Haul, R.; Gregg, S. J.; Sing, K. S. W. *Adsorption, Surface Area and Porosity*. In Berichte der Bunsengesellschaft für physikalische Chemie, 2nd ed.; Academic Press: London, 1982.
(49) Wakao, N.; Smith, J. M. Diffusion in catalyst pellets. *Chem. Eng. Sci.* **1962**, *17*, 825−834.
(50) Birkmann, F.; Pasel, C.; Luckas, M.; Bathen, D. Adsorption Thermodynamics and Kinetics of Light Hydrocarbons on Microporous Activated Carbon at Low Temperatures. *Ind. Eng. Chem. Res.* **2018**, *57*, 8023−8035.
(51) Yang, R. T. *Gas Separation by Adsorption Processes*; Elsevier Science, 2014.
(52) de Jong, A. M.; Niemantsverdriet, J. W. Thermal desorption analysis: Comparative test of ten commonly applied procedures. *Surf. Sci.* **1990**, *233*, 355−365.

https://doi.org/10.1021/acsomega.1c01994
ACS Omega 2021, 6, 16989−17001